

III-1

Accelerators and
Instruments

BL3U

Development of Resonant Soft X-ray Scattering for Soft Materials at UVSOR BL3U

H. Iwayama^{1,2} and T. Horigome¹¹UVSOR Synchrotron Facility, Institute for Molecular Science, Okazaki 444-8585, Japan²School of Physical Sciences, The Graduate University for Advanced Studies, SOKENDAI, Okazaki 444-8585, Japan

The liquid crystal is one of the most important materials for display devices. Their molecules have characteristic shapes such as rod and disc. This enables them to have both liquidity and symmetry of molecular alignments, which expresses interesting physical property such as a birefringence. In particular, chiral liquid crystal materials can have various kinds of phase, which are shown in Fig. 1. Depending on the phase, the sample is ferroelectric or anti-ferroelectric. In addition, they have intermediate phases between ferroelectric and anti-ferroelectric. To understand these physical properties, we need to know a periodic length of molecular layers, d . A typical value of d is from several nm to 100 nm. Since liquid crystal molecules mainly consist of light elements such as carbon, nitrogen and oxygen, resonant soft x-ray scattering is powerful tool.

We developed the equipment for resonant soft x-ray scattering (RSoXS) measurements. Figure 2 shows a schematic draw of an experimental setup. Our sample is S-MHPOBC and sandwiched between two 100 nm-Si₃N₄ membranes to avoid evaporations in a vacuum chamber. Sample can be heated up to 120 °C to observe various kinds of chiral smectic phases. Experiments were performed at UVSOR BL3U. Sample is irradiated with soft x-rays and scattering x-rays are detected by x-ray camera (Andor BN940P). We can measure scattering angles from 15° to 45°.

Figure 3 shows diffraction images at resonance and non-resonance photon energies and corresponding scattering angles. Here resonance is C 1s→ π^* core excitation, whose photon energy is $h\nu = 285$ eV ($\lambda = 4.3$ nm). For the resonance scattering, we found three ring structures at $y = -10, -4$ and 8 mm. At the resonance photon energy, intensities of ring structures at 8 mm strongly increase. By using Bragg's law, $d = \lambda/2\sin\theta$, we obtained d spectra for resonance and non-resonance. Here d is a periodic length, λ is a wavelength of photons, and 2θ is a scattering angle. We find peaks at $6.4, 9.7$ and 13.0 nm. Considering single molecular length of 3 nm, these peaks correspond to $2, 3$ and 4 molecular layer. Resonant enhancement of peak intensity for $d = 6.4$ nm suggests that the phase of the sample is anti-ferroelectric. Now we analyze the data in detail and investigate intermediate phases between ferroelectric and anti-ferroelectric one.

The RSoXS technique enables us to probe meso-scale (nm - μ m) structures with both elemental and chemical environment sensitivity and is ideal tool to study meso-scale materials such as polymer, block copolymer, composite morphology, particle assembly, organic

photovoltaic morphology, organic LEDs, membranes, porous materials, batteries and fuel cells, biomaterials, and so on [1].

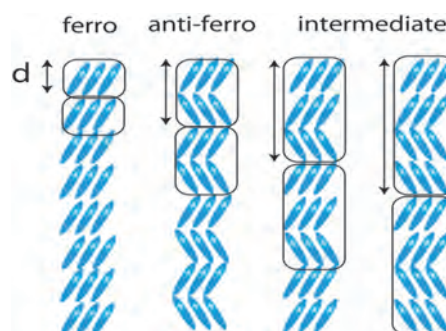


Fig. 1. Schematic view of molecular alignments for various kinds of chiral smectic phases.

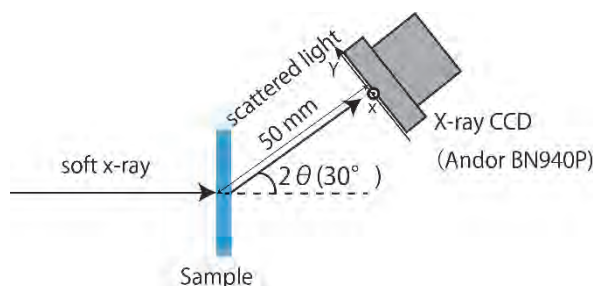


Fig. 2. Schematic draw of a new experimental setup for resonant soft x-ray scattering.

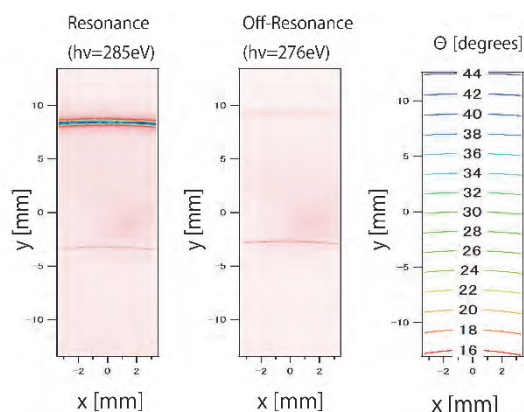


Fig. 3. Diffraction images for resonance and off-resonance and scattering angle map.

[1] F. Liu, M.A. Brady and C. Wang, *Eur. Polym. J.* **81** (2016) 555.

Others

Development of Nuclear Emulsion with Different Silver Halide Crystal Sizes for Cosmic-ray Imaging

A. Nishio, K. Morishima, K. Kuwabara, T. Yoshida and M. Nakamura
F-lab., Department of Physics, Nagoya University, Nagoya 464-8602, Japan

Cosmic ray imaging is the a new non-destructive inspection technique of large-scale constructions with cosmic ray muon. Cosmic ray muon has high penetrating power and it always comes from the whole sky. In the same way of taking a X-ray photograph, we can obtain integrated density of constructions which thickness are several tens cm to several km. We had ever applied this technique to the pyramid of khufu at Egypt, and discovered a large void [1].

In cosmic-ray imaging observations, we used nuclear emulsion as a detector. Nuclear emulsion is a kind of photographic film and has sensitivity for ionizing radiation. The film records tracks of charged particle with angular accuracy under several mrad. In Nagoya University, started a emulsion gel production machine in 2010. It was enabled us to develop new-type emulsion gel by ourselves.

We have succeeded to develop the Large crystal Nuclear Emulsion and the relationship between the size of silver halide crystals in nuclear emulsion and their sensitivity to the minimum ionized particles was investigated.

Gold-sulfur-sensitized silver iodobromide crystals with a diameter of approximately 180 - 540 nm were prepared (Fig.1), and their photo sensitivity and minimum ionized particle sensitivity were investigated.

First, we confirmed that the photo sensitivity was proportional to the crystal volume and that the quantum sensitivity to light was sufficiently high (Fig. 2).

After that, minimum ionized particle sensitivity was investigated (Fig. 3). The grain density was found to be 1.3 to 1.4 times higher with the same volume occupancy of crystals by increasing the crystal size to 400 nm in diameter than the conventional size of 220 nm. It was also found that the grain density could not be significantly increased due to the decrease in the number of crystals, even if the crystal size was larger than 400 nm.

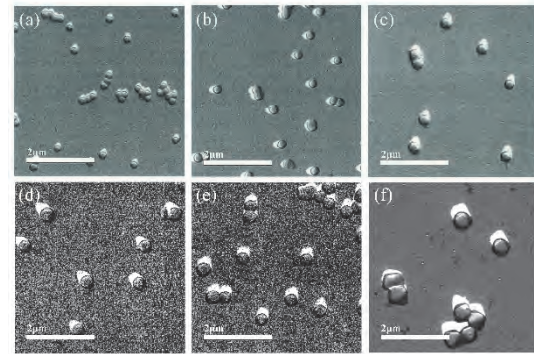


Fig. 1. EM images of silver halide crystals of different sizes.

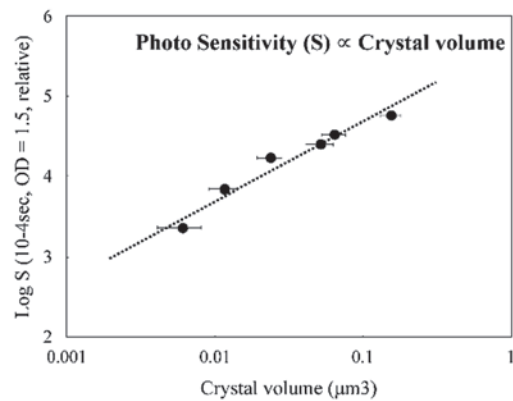


Fig. 2. Relationship between photo sensitivity S (relative value) and crystal volume.

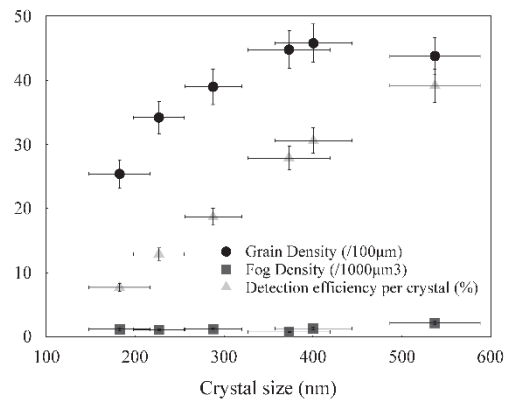


Fig. 3. Crystal size dependence of sensitivity to the minimum ionized particles; Grain density, Fog density, and detection efficiency per crystal.

[1] K. Morishima *et al.*, Nature **552** (2017) 386.

Survey of Low Emittance Optics for UVSOR-III

E. Salehi¹ and M. Katoh^{1,2}

¹UVSOR Synchrotron Facility, Institute for Molecular Science, Okazaki 444-8585, Japan

²Hiroshima Synchrotron Radiation Center, Hiroshima University, Higashi-Hiroshima 739-0046, Japan

This is a study on a future plan of UVSOR synchrotron to provide diffraction-limited light in the vacuum ultraviolet range. For this purpose, the small emittance less than at 1 nm is required. UVSOR is a low energy synchrotron light source. After some major upgrades [1-4], it is now called UVSOR-III, which has a moderately small emittance of about 17 nm and provide vacuum ultraviolet light of high brightness.

As the first step of the study, we have analyzed the present magnetic lattice of UVSOR III to seek a possible low emittance without major changes of the lattice. We draw a “tie diagram” of UVSOR III as shown in Fig.1, which indicates the quadrupole parameter region where a periodic solution exists, as well as the emittance of each parameter set is shown by the color. In reality, UVSOR-III has four quadrupole families. However, to draw the tie diagram, they are grouped into two families (QF and QD) located symmetrically around the bending magnets. The code, Elegant [5], was used and the two quadrupole strengths are surveyed. Figure 1 shows that there are a few areas which has significantly smaller emittance around 10 nm than the present value, 17 nm. However, there seems no solution which gives the emittance much smaller than 10 nm. The hardware limitations of the quadrupole field strengths are indicated in the figure. For the operation energy, 750 MeV, a part of the low emittance region is out of the limitation. However, if the machine is operated at 600 MeV, most of the low emittance area is within the limitation. It should be noted that the emittance is proportional to the square of the electron energy, the low energy operation would give even smaller emittance.

On the tie diagram, we can find some solutions which give a smaller emittance than the present value. Making these parameters as the initial values for four quadrupole families, we designed some optics which may be worth to investigate further. The optic presented in Fig. 2 has an emittance smaller than 10 nm at the electron energy, 750 MeV. In this optics, the vertical betatron function at the straight sections are not as small as the present optics. Therefore, this optics may not be compatible with the operation of the narrow gap undulators. In some special studies which requires a small emittance as possible, this optics may be useful. Another interesting optic is shown in Fig. 3, which gives a small emittance, 13 nm, with a fewer numbers of quadrupoles. In this optics, we can remove one quadrupole family at the short straight sections. This may be beneficial to install new devices for beam handlings, beam monitors or light source developments.

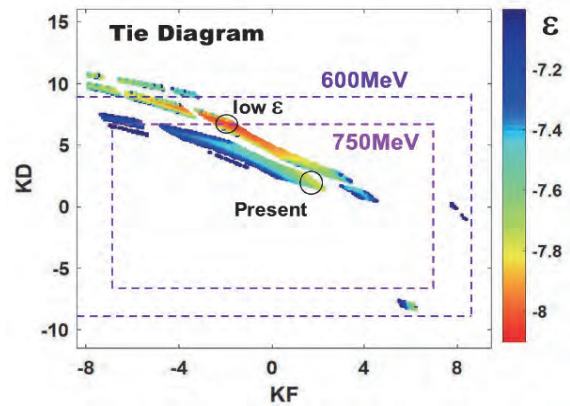


Fig. 1. Tie diagram of UVSOR-III magnetic lattice. KF and KD are quadrupole strengths.

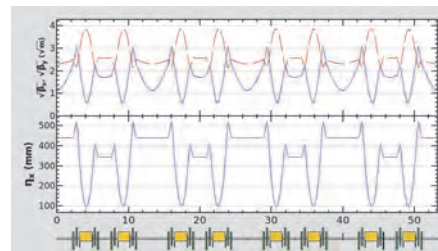


Fig. 2. An optic with a small emittance of 9.4 nm at 750 MeV.

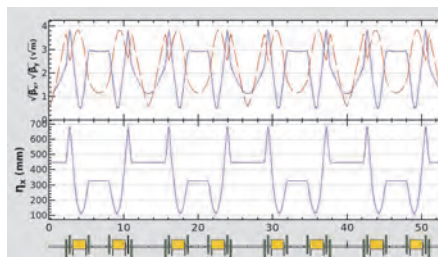


Fig. 3. An optic which gives a moderately small emittance of 13.3 nm with less numbers of quadrupoles.

- [1] M Katoh, K Hayashi, *et al.*, Nucl. Instr. Meth. A **467** (2001) 68.
- [2] M Katoh, M Hosaka, *et al.*, AIP Conf. Proc. **705** (2004) 49.
- [3] M Adachi, H Zen, *et al.*, J. Phys. Conf. Ser. **425** (2013) 04201.
- [4] M. Katoh, M. Adachi, *et al.*, AIP Conf. Proc. **1234** (2010) 531.
- [5] M. Borland, APS LS-287 (2000).
<https://www.aps.anl.gov/Accelerator-Operations-Physics/Software>

BL1U

Selective Isotope 3D-CT Imaging in UVSOR-BL1U

H. Ohgaki¹, K. Ali¹, H. Zen¹, T. Kii¹, T. Hayakawa², T. Shizuma², H. Toyokawa³,
M. Fujimoto⁴, Y. Taira⁴ and M. Katoh^{4,5}

¹Institute of Advanced Energy, Kyoto University, Uji 611-0011, Japan

²Tokai Quantum Beam Science Center, National Institutes for Quantum and Radiological Science and Technology, Tokai-mura 319-1106, Japan

³National Institute of Advanced Industrial Science and Technology (AIST), Tsukuba 3058568, Japan

⁴UVSOR Synchrotron Facility, Institute for Molecular Science, Okazaki 444-8585, Japan

⁵Hiroshima University, Higashi-Hiroshima 739-8511, Japan

A Nuclear Resonance Fluorescence (NRF) method is a powerful tool for investigating nuclear physics and isotope imaging inside the spent nuclear fuel canisters and nuclear wastes. We have been developing an isotope imaging technique using the NRF scattering method in AIST [1] and transmission method in UVSOR-III [2].

We successfully got 2D NRF-CT images by using an LCS gamma-ray beam with two enriched isotope targets, ²⁰⁶Pb (>93.3 %) and ²⁰⁸Pb (>97.8 %), inserted in an aluminum holder at the beamline BL1U in UVSOR-III in 2019 [3]. In 2020, we tried to obtain a 3D image of the same CT target. The geometry of the CT target is shown in Fig. 1.

The LCS gamma-ray beam with a maximum energy of 5.528 MeV was generated by using a fiber laser (wavelength of 1,896 μm, 50 W). The gamma-ray beam with a 10 photon · s⁻¹ · eV⁻¹ flux density was used to excite J^π=1⁻ state at 5.512 MeV of ²⁰⁸Pb with a 2-mm lead collimator. The gamma-ray absorption by the CT target was measured at 4-mm step in the horizontal direction (x= -12 to +12 mm) and 30° step in the rotation angle (θ=0° to 150°). Three vertical positions (z=3, 11, and 17 mm from the holder's bottom) were taken. Two HP-Ge detectors measured the NRF signals from the witness target (²⁰⁸Pb enriched) with 100 % and 130 % relative efficiencies. The transmission gamma-rays have been measured by a 3.5" × 4" LaBr₃(Ce) detector, which gives a density distribution by the atomic absorption process of the sample target at the same time. After suppressing the atomic absorption process measured by the LaBr₃(Ce) detector, the NRF-CT images, which selectively indicate the distributions of ²⁰⁸Pb, were obtained. Figure 2 shows a typical one-layer CT image (z=3 mm case). By stacking 3-layer NRF-CT images, a rough 3D NRF-CT image of ²⁰⁸Pb distribution in the CT target was successfully obtained, as shown in the Fig. 3.

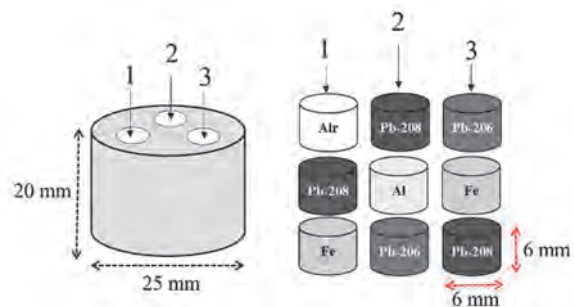


Fig. 1. Geometry of the CT target. Right figure shows the configuration of enriched rods inserted to the aluminium cylinder shown in the left figure.

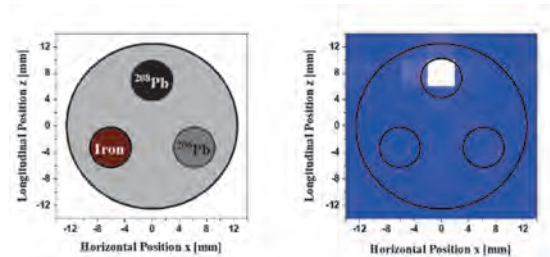


Fig. 2. NRF-CT image at z= 3 mm

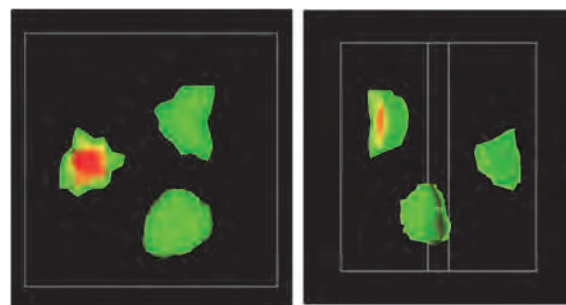


Fig. 3. 3D NRF-CT image

[1] N. Kikuzawa *et al.*, Appl. Phys. Express **2** (2009) 036502.
[2] H. Zen *et al.*, AIP Advances **9** (2019) 035101.
[3] K. Ali *et al.*, IEEE Trans. Nucl. Sci. **67** (2020) 1976.

BL1U

Elastic Scattering of Gamma-rays with Energies of 10 MeV

T. Hayakawa¹, K. Kawase¹, T. Shizuma¹, R. Hajima¹, J. K. Koga², H. Zen³, T. Kii³,
H. Ohgaki³, M. Fujimoto⁴, Y. Taira⁴ and M. Katoh^{4,5}

¹National Institutes for Quantum and Radiological Science and Technology, Tokai-mura 319-1106, Japan

²National Institutes for Quantum and Radiological Science and Technology, Kizugawa 619-0215, Japan

³Institute of Advanced Energy, Kyoto University, Kyoto 611-0011, Japan

⁴UVSOR Synchrotron Facility, Institute for Molecular Science, Okazaki 444-8585, Japan

⁵Hiroshima University, Higashi-Hiroshima 739-8511, Japan

QED theory predicted unresolved nonlinear effects such as photon-photon interactions [1,2]. Recently, virtual photon – virtual photon scattering with energies of 5 TeV has been measured using a high energy accelerator [1]. One of the photon-photon interactions is Delbrück scattering, which is an elastic scattering of gamma-rays. However, there was a critical problem that one cannot calculate the scattering using only the amplitude of Delbrück scattering due to the interference of other elastic scattering. Koga and Hayakawa [3] have presented that it is possible to measure selectively the amplitude of Delbrück scattering using linearly polarized gamma-rays.

To study Delbrück scattering we have installed a CO₂ laser [4]. Here, we have installed a fiber laser with a wavelength of 1064 nm and an average power of 10 W. The pulse width is 1 ns and the pulse energy is 25 μJ. The maximum repetition is 400 kHz and can be controlled by an external trigger. The laser Compton scattering (LCS) gamma-rays with a maximum energy of 10 MeV were generated by interactions with electron beams having an energy of 750 MeV stored in UVSOR-III. To generate linearly polarized gamma-rays we used a linear polarized laser. We newly developed a collimator system and detector frame. The tungsten target with a diameter of 5 mm and a length of 50 mm was used. The gamma-rays scattered from the target were measured with two 3.5'' × 4'' LaBr₃(Ce) scintillation detectors, which were placed at $\phi = 0$ and 90 degrees from the linear polarization plane at $\theta = 90$ degrees away from the gamma-ray propagation axis (see Fig. 1). Figure 2 shows the measured energy spectra. A broad peak is observed in an energy region from 5–7 MeV in Fig. 2(b) but it is not observed in Fig. 2(a). This peak originates from Compton scattering on a mirror inside the beamline. The elastic scattering is not clearly observed.

[1] ATLAS Collaboration, *Nature Physics* **13** (2017) 852.

[2] T. Inada, *et al.*, *Phys. Lett. B* **732** (2014) 356.

[3] J. K. Koga and T. Hayakawa, *Phys. Rev. Lett.* **118** (2017) 204801.

[4] H. Zen *et al.*, *J. Phys.: Conf. Ser.* **1067** (2018) 092003.

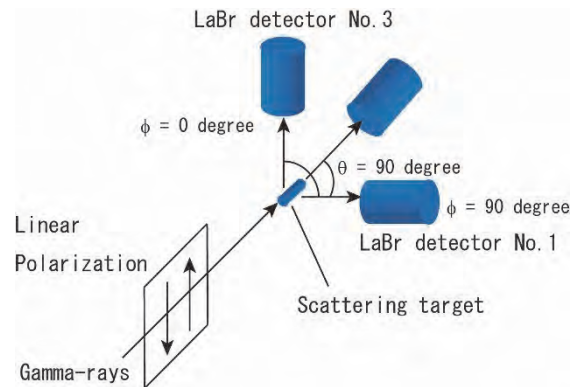


Fig. 1. A schematic view of the scattering experiment. The gamma-rays scattered from the target were measured with two LaBr₃(Ce) scintillation detectors.

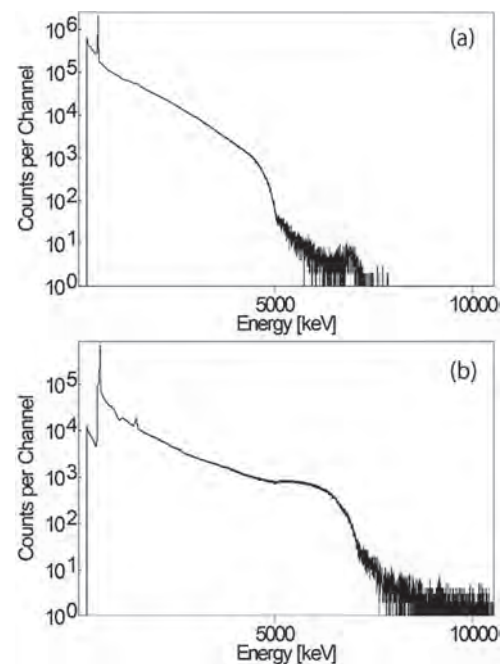


Fig. 2. Measured gamma-ray spectra using LaBr₃(Ce) scintillation detectors. The spectrum measured at $\phi = 0^\circ$ away from the linear polarization plane (a) and that at $\phi = 90^\circ$ (b).

BL1U

Improvement of Interferometer for Measuring The Coherence Length of Light from an Undulator

A. Mano¹, S. Kimura¹, M. Hosaka¹, T. Takashima¹ and M. Katoh^{2,3}

¹Nagoya University, Nagoya 464-8603, Japan

²Hiroshima University, Higashi-Hiroshima, 739-0046, Japan

³UVSOR Synchrotron Facility, Institute for Molecular Science, Okazaki 444-8585, Japan

We are experimentally studying the time domain structure of light from an undulator so-called coherence length, which is wave packet length emitted from a single electron passing through the undulator.

We attempted to measure the coherence length of light from an undulator using a Michelson-type interferometer [1]. The light from the undulator is split by the first beam splitter (non-polarizing type). After split lights are folded back by the retroreflector and overlapped again by the second beam splitter. By moving one of the retroreflectors, a difference in the optical path is created. The overlapping lights interfere with each other, causing fluctuation in intensity according to the optical path difference. The intensity fluctuation is called an interferogram. If the overlapping light is angled, the image forms interference fringes, but the interferogram corresponds to the intensity fluctuation of a single point in the image. The interferogram is the autocorrelation of the undulator light wave packet.

At first, we constructed an interferometer using $\phi 20$ mm pedestal posts. We use 10 mm square cube type beam splitters and right-angle prisms as retroreflectors. This interferometry is shown in Fig.1. This optical system generated a lot of stray light and was difficult to adjust. Further, this optical system had low rigidity and the optical elements were prone to vibration. The system was exposed, therefore it was easily affected by fluctuations in the atmosphere. The image of the interference fringes obtained by this optical system is shown in Fig. 2. In Fig. 2. (b), the fringes are blurred, probably due to vibration. In Fig. 2. (c), the phase of the fringes is shifted, probably due to atmospheric fluctuations. Thus, the interferogram measurement proved to be very difficult with this optical system.

We attempted to improve the interferometer. By changing the single-point support of the pedestal post to multi-point support by the optical cage system, the rigidity of the system has been improved and rough alignment is no longer necessary. To reduce stray light, the beam splitter cube was replaced with a beam splitter plate and the retroreflector was replaced with two mirrors. Further, the use of a kinematic holder for the folded mirror made it easier to adjust the overlay of the two split beams. Furthermore, by covering the area around the optical system, it was protected from atmospheric fluctuations. These improvements made it possible to obtain stable images of interference fringes.

More details on the results from the improved

interferometer will be presented in a future paper.



Fig. 1. Photo of the interferometer we first constructed.

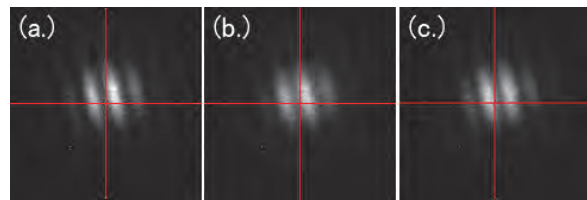


Fig. 2. Images of interference fringe in the same condition.

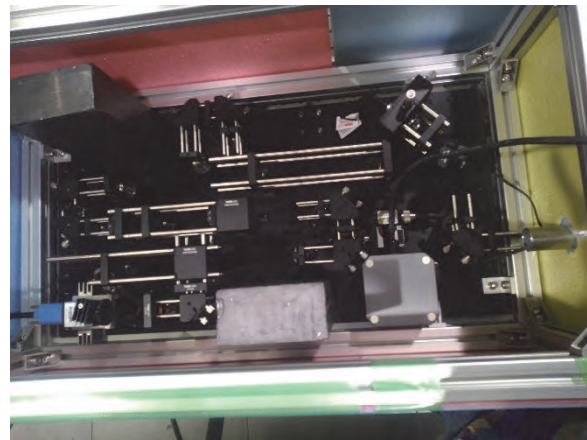


Fig. 3. Photo of the improved interferometer.

[1] S. Notsu *et al.*, UVSOR Activity Report 2019 47 (2020) 37.

BL2A

Evaluation of the Robustness of Back-illuminated CMOS Sensors Against Soft X-rays

N. Narukage

National Astronomical Observatory of Japan, Mitaka 181-8588, Japan

The solar corona is full of dynamic phenomena. They are accompanied by interesting physical processes, namely, magnetic reconnection, particle acceleration, shocks, waves, flows, evaporation, heating, cooling, and so on. The understandings of these phenomena and processes have been progressing step-by-step with the evolution of the observation technology in EUV and X-rays from the space. But there are fundamental questions remain unanswered, or haven't even addressed so far. Our scientific objective is to understand underlying physics of dynamic phenomena in the solar corona, covering some of the long-standing questions in solar physics such as particle acceleration in flares and coronal heating. In order to achieve these science objectives, we identify the imaging spectroscopy (the observations with spatial, temporal and energy resolutions) in the soft X-ray range (from ~ 0.5 keV to ~ 10 keV) is a powerful approach for the detection and analysis of energetic events [1]. This energy range contains many lines emitted from below 1 MK to beyond 10 MK plasmas plus continuum component that reflects the electron temperature.

The soft X-ray imaging spectroscopy is realized with the following method. We take images with a short enough exposure to detect only single X-ray photon in an isolated pixel area with a fine pixel Silicon sensor. So, we can measure the energy of the X-ray photons one by one with spatial and temporal resolutions. When we use a high-speed soft X-ray camera that can perform the continuous exposure with a rate of more than several hundred times per second, we can count the photon energy with a rate of several 10 photons / pixel / second. This high-speed exposure is enough to track the time evolution of spectra generated by dynamic phenomena in the solar corona, whose lifetimes are about from several ten seconds to several minutes.

For the first imaging spectroscopic observation of the solar corona in soft X-ray range, we launched a NASA's sounding rocket (FOXSI-3) on September 7th, 2018 and successfully obtained the unprecedented data [2] using a high-speed X-ray camera [3] with a back-illuminated CMOS sensor [4].

Though this back-illuminated CMOS sensor has an enough photon-counting capability for the X-ray imaging-spectroscopy as demonstrated by FOXSI-3 flight, we found that it is damaged by the incident X-rays (which themselves are the targets of detection) as shown in Fig. 1.

For the evaluation of the robustness of the sensor against the incident X-rays, we did the following

procedures:

1. Take dark image to monitor the dark level (bias level) and noise level (readout noise + dark noise).
2. Emit the monochromatic intense X-rays with BL2A for a certain period.
3. Repeat Procedures 1 and 2 until the dark level is saturated.

We did this evaluation with three monochromatic X-rays of 1 keV, 2 keV and 4 keV, for two types of back-illuminated CMOS sensors, whose difference is only the thickness of sensitive layers. The thicknesses are about $4\mu\text{m}$ and $10\mu\text{m}$. Based on these evaluations, we found that the sensor with the thicker sensitive layer can survive against the more incident X-ray photons. In the energy of each monochromatic X-rays, the detectable X-ray photon number without serious damage is roughly proportional to the absorption rate of the sensitive layer. Hence, we suspected that the presumable damaged part is the circuit layer, which is located behind the sensitive layer.

In our estimate based on these evaluations, more than $\sim 15\mu\text{m}$ sensitive later is required for solar flare observations. We plan to confirm this result using the CMOS sensor with $25\mu\text{m}$ sensitive layer in FY2021.

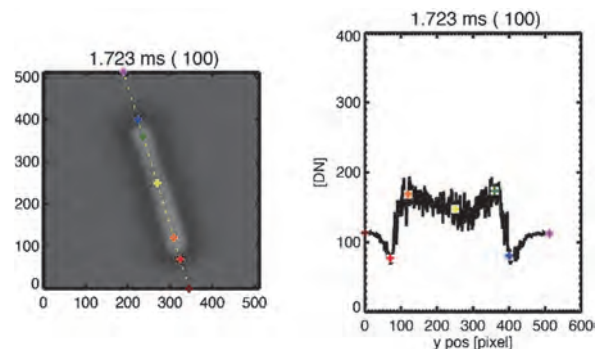


Fig. 1. Dark image of the CMOS damaged by X-rays.

[1] N. Narukage *et al.*, White paper of the “soft X-ray imaging spectroscopy”, arXiv:1706.04536 (2017).

[2] N. Narukage and S. Ishikawa, UVSOR Activity Report 2018 **46** (2019) 36.

[3] S. Ishikawa *et al.*, Nuclear Instruments and Methods in Physics Research Section A **912** (2018) 191.

[4] N. Narukage *et al.*, Nuclear Instruments and Methods in Physics Research Section A **950** (2020) 162974.

BL3U

Development of an Ultrathin Liquid Cell for Soft X-ray Absorption Spectroscopy in the Low-Energy Region

M. Nagasaka^{1,2}¹Institute for Molecular Science, Okazaki 444-8585, Japan²The Graduate University for Advanced Studies, SOKENDAI, Okazaki 444-8585, Japan

Soft X-ray absorption spectroscopy (XAS) is an element-specific method to investigate local structures of liquids and solutions. Recently, we have developed a transmission-type liquid cell for XAS of liquid samples, where a liquid layer is sandwiched between two Si_3N_4 membranes with the thickness of 100 nm and the liquid thickness is precisely controlled by adjusting the helium pressure around the liquid cell [1]. On the other hand, the low-energy region below 200 eV is important for chemical research since it includes K-edges of Li and B and L-edges of Si, P, S, and Cl. However, the soft X-ray transmission calculation [2] predicts that soft X-rays below 200 eV cannot transmit the present liquid cell, which consists of four Si_3N_4 membranes and 20 mm optical path of He gas. Recently, we have established the argon gas window, which is effective for the transmission of soft X-rays from 60 to 240 eV with the removal of high order X-rays [3]. We also found that soft X-rays in the low-energy region can transmit the ultrathin liquid cell with the optical length of 2.6 mm. In this study, we realize XAS in the low-energy region by developing the ultrathin liquid cell.

Figure 1(a) shows a schematic of the XAS measurement system including the ultrathin liquid cell. The experiment was performed at BL3U. In the ultrathin liquid cell, a liquid layer is sandwiched between two Si_3N_4 membranes and is in an atmospheric Ar condition. The soft X-ray beamline and a photodiode detector are under ultrahigh vacuum conditions and are separated from the atmospheric Ar chamber with Si_3N_4 membranes with a small window size ($0.2 \times 0.2 \text{ mm}^2$). Figure 1(b) shows photographs of the ultrathin liquid cell. In the left part, soft X-rays pass through the Si_3N_4 membranes settled in the center part of the liquid cell. In the right part, the thickness of the ultrathin liquid cell becomes 2.4 mm. Considering the thickness of the holders of small Si_3N_4 windows, the optical pass length of Ar gas is estimated to be 2.6 mm.

Figure 2 shows Cl L-edge XAS spectrum of 2 M LiCl solution by using the ultrathin liquid cell. The spectrum shows two peaks with the positions of 203 eV and 208 eV. We have also obtained Li K-edge XAS spectrum of 2 M LiCl solution although the signal-to-noise ratio is not sufficient due to the low photon flux at the Li K-edge. In the present study, we have confirmed the effectiveness of the ultrathin liquid cell for XAS in the low-energy region. However, the photon flux is still low due to the strong absorption of Si_3N_4 membranes at the Si L-edge (100 eV). It is difficult to optimize the absorbance of solute LiCl peaks with the increase of the

liquid thickness. In the future, we will prepare polymer membranes that consist of no Si atoms to obtain high photon flux of transmitted soft X-rays and measure XAS spectra in the low-energy region with a good signal-to-noise ratio.

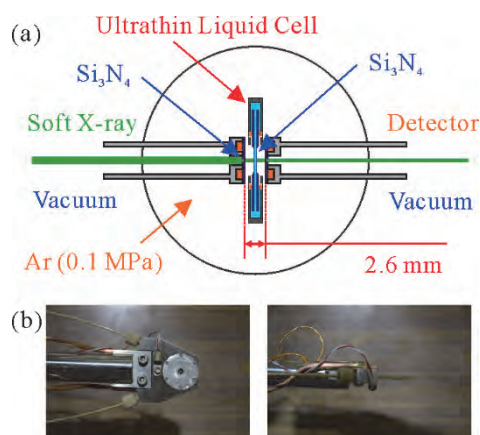


Fig. 1. (a) A schematic of the XAS measurement system in the low-energy region with the ultrathin liquid cell. (b) Photographs of the ultrathin liquid cell.

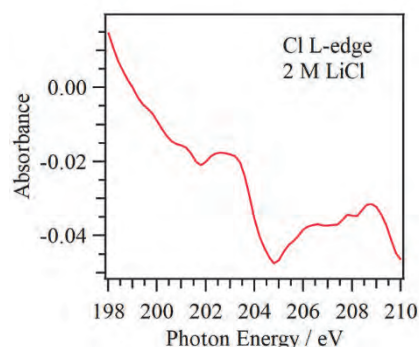


Fig. 2. Cl L-edge XAS of 2 M LiCl solution.

[1] M. Nagasaka, H. Yuzawa and N. Kosugi, *Anal. Sci.* **36** (2020) 95.

[2] C. T. Chantler, *J. Phys. Chem. Ref. Data* **29** (2000) 597.

[3] M. Nagasaka, *J. Synchrotron Rad.* **27** (2020) 959.

BL3B

Development of Ion Time-of-Mass Spectrometer at UVSOR BL3B

H. Iwayama^{1,2} and T. Horigome¹

¹UVSOR Synchrotron Facility, Institute for Molecular Science, Okazaki 444-8585, Japan

²School of Physical Sciences, The Graduate University for Advanced Studies, SOKENDAI, Okazaki 444-8585, Japan

Halogenated alkanes are used as flame retardants, fire extinguishants and refrigerant gases. While they are useful and widely used in commerce, they have also been shown to be serious pollutants and toxins. In particular, the chlorofluorocarbons have been shown to lead to ozone depletion. Photolysis and the reactions of these substances with hydroxyl radical, the main oxidizing agent of the troposphere, derived from the photolysis of ozone, determine their life-time in the atmosphere. In the stratosphere they interact with VUV light and produce halogen atoms which contribute to the ozone depletion process. Photodissociation and photoionization channels are very interesting since different fragmentation channels can lead to different radical and/or cations which can play a role in several fields, from atmospheric chemistry to etching and plasma assisted industrial process. In this work, we developed ion time-of-flight mass spectrometer at BL3B for photochemistry of halogenated alkanes in UV and VUV region.

The experiment was performed at UVSOR BL3B, where we use intense synchrotron light from visible to EUV regions. A schematic view of our experimental setup is shown in Fig. 1. The sample gas jet is generated from the capillary nozzle and irradiated by VUV light between ion and electron extract meshes. While a photoelectron is detected by the electron MCP detector, an ion is introduced to ion time-of-flight mass spectrometer. Detection signals of electron and ion are used as start and stop signal for time-of-flight spectrometer, respectively. The sample is R22 gases (CHF_2Cl).

Figure 2 shows ion time-of-flight mass spectra for CHF_2Cl molecules at photon energies of 15, 20 and 30 eV. At the photon energy of 15 eV, we find that dominant fragment ions are CHF_2^+ . This means that major photodissociation is $\text{CHF}_2\text{Cl} + h\nu (15\text{eV}) \rightarrow \text{CHF}_2^+ + \text{Cl}$ and generate a Cl radical. Here we note that relative abundance of parent molecular ions, CHF_2Cl^+ , is very low. Our results suggest that the C-Cl bond is easily broken by VUV photon absorptions. By increasing photon energies, we also find smaller fragment ions such as CF^+ , Cl^+ and CH^+ and H^+ ions. Since we also measured these ion yields as a function of photon energies, corresponding appearance energies of each fragment ions will be deduced. Now we analyzed these results in details.

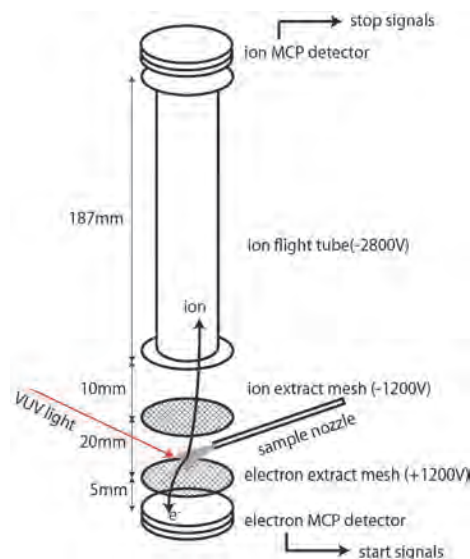


Fig. 1. Schematic view of our ion time-of-flight spectrometer.

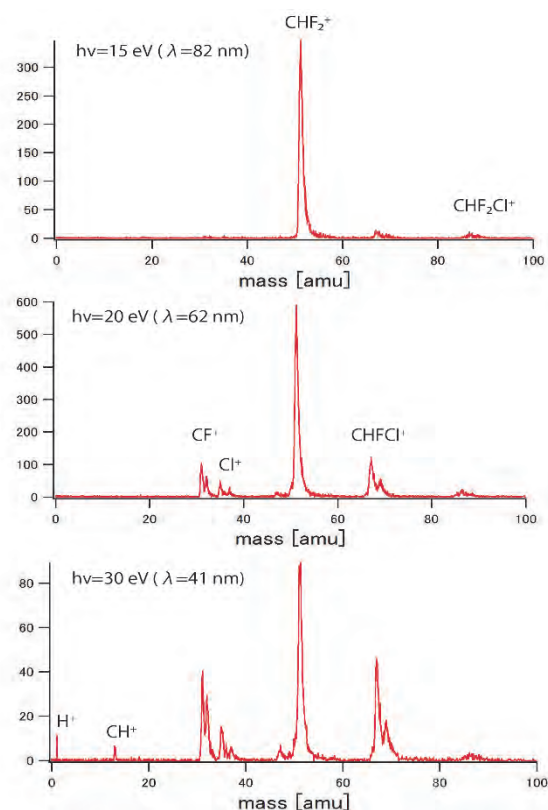


Fig. 2. Ion time-of-flight mass spectra for CHF_2Cl molecules at photon energies of 15, 20 and 30 eV.

BL4U

Study of STXM with IR Laser Optics Part I. – In-Situ Removal of Organic Contamination from Carbon Nanotube –

H. Yuzawa¹ and T. Ohigashi^{1,2}¹UVSOR Synchrotron Facility, Institute for Molecular Science, Okazaki 444-8585, Japan²School of Physical Sciences, The Graduate University for Advanced Studies, SOKENDAI, Okazaki 444-8585, Japan

Scanning Transmission X-ray Microscope (STXM) gives two-dimensional X-ray absorption spectroscopy (XAS) spectra of sample with ca. 50 nm spatial resolution, which is powerful to get the distribution of chemical state. However, the measurement immediately after heating sample in the STXM chamber is difficult because the focal length of a Fresnel zone plate (FZP) in soft X-ray region is short as shown in Fig. 1a. Main problems of this measurement are harmful influences for the optical elements, and large sample drift by thermal vibration. In the present study, we have carried out heating the sample by using an IR laser diode from outside of the chamber to reduce the remaining thermal source in there. As a test sample for heating, carbon nanotube (CNT) has been applied to in-situ removal of its organic contaminations, based on the user's request.

Figure 1b shows the picture of experimental set up for heating the sample. Diverging light of the multimode IR laser diode (3 W, 940 nm) is collimated with two cylindrical plane-convex lenses ($f = 5$ and 10 cm) and is focused to sample inside the STXM chamber with a spherical plane-convex lens ($f = 50$ cm).

CNT (NanoIntegrus Inc., IsoNanotube-S) was used as the sample, whose contaminations are iodixanol (Fig. 2) and some surfactant (its structure is not open) [1]. 0.5 mg of the CNT was dispersed into water (40 ml) by using an ultrasonic homogenizer, then the suspension (3 μ l) was dropped and dried on a Si₃N₄ membrane (window size, 0.5 \times 0.5 mm²). STXM measurements in C *K*-edge of the CNT were carried out after heating the sample at ca. 280 °C under vacuum for 15 min. During the heating of the sample, the sample and a detector stage were moved to 7 cm backward from its measuring position.

Figure 3a shows one of the STXM images of aggregated CNT in C *K*-edge XAS measurement. The drift of sample is at most 200 nm during the measurement. Since this value is enough small for basic measurements in BL4U, the harmful influence of the thermal source is successfully reduced by using the IR laser diode. Figure 3b shows the corresponding C *K*-edge XAS spectra. The spectral shape is gradually changed with increasing the integrated irradiation time of the IR laser. All the measuring region of CNT in Fig. 3a converges to the reported spectrum of it [2] for 75 min (Fig. 3b, blue line).

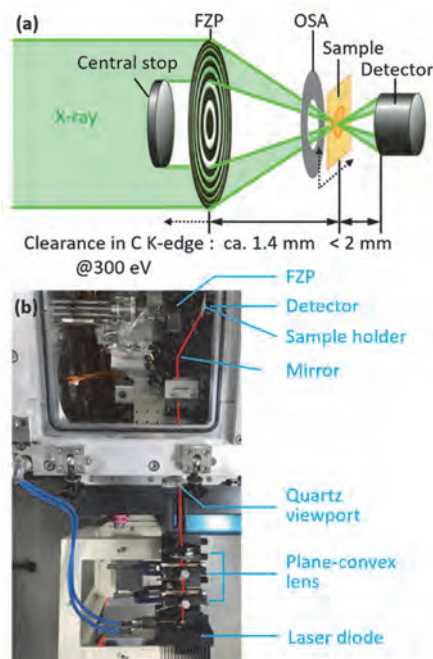


Fig. 1. (a) Side view of optical system around the sample in STXM chamber. Dotted-line arrows show the moving direction during measurements. (b) Top view of optical system for heating the sample by IR laser diode.

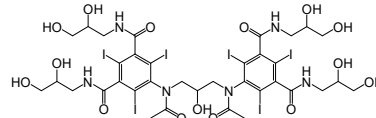


Fig. 2. Structural formula of iodixanol.

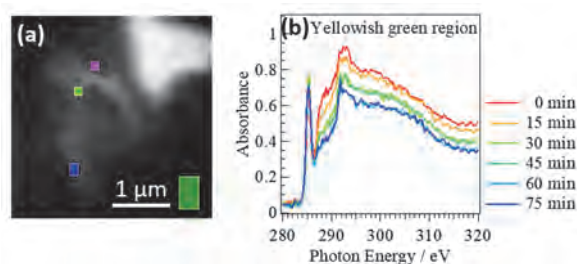


Fig. 3. (a) STXM image (based on absorbance [$= -\ln(I/I_0)$]) of aggregated CNT at 290 eV. I_0 was taken from green region. (b) C *K*-edge XAS spectra of yellowish green region in (a), measured every 15 min irradiation of the IR laser.

[1] Homepage of NanoIntegrus Inc.

[2] S. Banerjee *et al.*, *J. Phys. Chem. B* **109** (2005) 8489.

BL4U

Study of STXM with IR Laser Optics Part II. – In-Situ Observation of Mn₂O₃ Calcination –

H. Yuzawa¹ and T. Ohigashi^{1,2}¹UVSOR Synchrotron Facility, Institute for Molecular Science, Okazaki 444-8585, Japan²School of Physical Sciences, The Graduate University for Advanced Studies, SOKENDAI, Okazaki 444-8585, Japan

Defect formation in solid is an attractive research field in such as material chemistry and catalytic chemistry. For example, the defect in the photocatalyst influences photocatalytic activity and product selectivity [1]. Thus, the observation of defect formation is important under various conditions (e.g., temperature and pressure) of sample.

Scanning Transmission X-ray Microscopy (STXM) is powerful analytical method to get the two-dimensional distribution of chemical state. In the previous page of this activity report [2], we reported the thermal treatment of the CNT to remove the organic contaminations by using the IR laser diode. In the present study, we have applied this system to the observation of defect formation in Mn₂O₃ sample, which is one of the famous oxide catalysts.

Experiments were performed in the BL4U connected with the optical system of IR laser diode (see the Fig. 1(b) of [2]). 10 mg of Mn₂O₃ (Wako Pure Chemical Industries, Ltd.) was dispersed into 50 ml water with vigorous stirring, then the suspension (3 μ l) was dropped and dried on a Si₃N₄ membrane (window size, 1 \times 1 mm²). STXM measurements in O *K*-edge and Mn *L*-edge were carried out after heating the sample at ca. 300 °C under vacuum for 10 s. During the heating of the sample, the sample and a detector stage were moved to 7 cm backward from its measuring position.

Figure 1(a) shows the representative STXM image of aggregated Mn₂O₃ particles in Mn *L*-edge XAS measurement before the heating. Through the entire measurement (10 cycles of the IR laser radiation (100 s) and 11 cycles of STXM measurements for O *K*-edge (5.5 h) and Mn *L*-edge (6.5 h)), the sample shape was almost the same as that in Fig.1(a). On the other hand, in Figs. 1(b) and 1(c), both O *K*-edge and Mn *L*-edge XAS are varied with increasing the integrated heating time until 50 s, and then almost the constant spectra are obtained from 60 to 100 s. The finally obtained spectra of O *K*-edge and Mn *L*-edge are similar to those of Mn₃O₄ [3]. Thus, this spectral change indicates that the defect of oxygen is produced in Mn₂O₃ and the valence of Mn partially changed from III to II during the heating.

In another run of measurement, the influence of soft X-ray radiation on the state of Mn₂O₃ without heating was evaluated (Figure is not shown). As the result of 3 cycles of STXM measurement in O *K*-edge and Mn *L*-edge under vacuum at room temperature, the sample shape and the spectra did not change. This result indicates that any change of state in Figs. 1(b) and 1(c)

is not derived from soft X-ray radiation but the heating of sample.

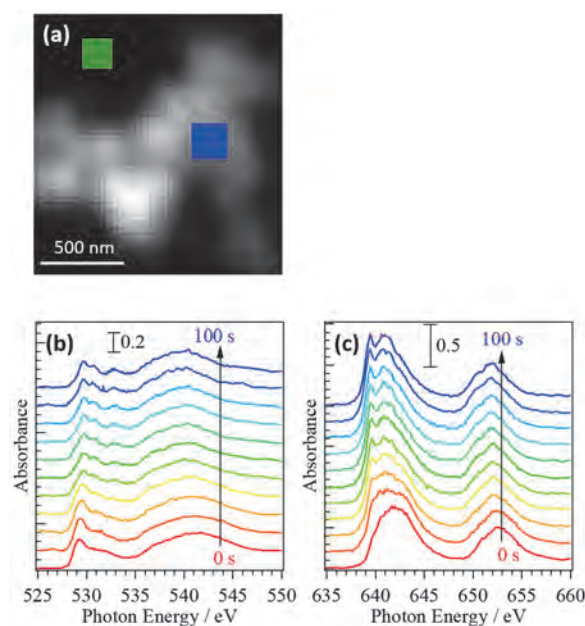


Fig. 1. (a) STXM image (based on absorbance [$= -\ln(I/I_0)$]) of aggregated Mn₂O₃ particles at 640 eV. I_0 was taken from green region. (b) O *K*-edge XAS spectra and (c) Mn *L*-edge XAS spectra of the blue region of (a), measured every 10 s IR laser radiation.

- [1] S. A. Rawool *et al.*, Chem. Sci. **12** (2021) 4267.
 [2] H. Yuzawa and T. Ohigashi, UVSOR Activity Report 2020 **48** (2021) 42.
 [3] B. Gilbert *et al.*, J. Phys. Chem. A **107** (2003) 2839.

BL4B

Development of High Efficiency Liquid Cell in Total Electron Yield Using Atomically-thin Graphene

I. Mitsuishi¹, K. Kashiwakura¹, Y. Niwa¹, T. Ogawa¹, Y. Tawara¹, R. Kitaura², P. Solís-Fernández³, K. Kawahara³, H. Ago³, T. Taniguchi⁴, K. Nomoto⁴, H. Kodaka⁴, T. Horigome⁵, E. Nakamura⁵, H. Iwayama⁵, M. Nagasaka⁵ and K. Tanaka⁵

¹Graduate School of Science, Division of Particle and Astrophysical Science, Nagoya University, Nagoya 464-8602, Japan

²Department of Chemistry, Nagoya University, Nagoya 464-8602, Japan

³Global Innovation Center, Kyushu University, Kasuga, 816-8580, Japan

⁴Optical Measurement Technology Development Department, R&D Division, USHIO INC., Yokohama 225-0004, Japan

⁵UVSOR Synchrotron Facility, Institute for Molecular Science, Okazaki 444-8585, Japan

X-rays are a powerful probe to investigate material properties through, e.g., X-ray absorption spectroscopy (XAS) which can reveal local atomic and electronic states of oxygen, carbon, etc.. Among the XAS methods for liquid, total electron yield is preferably utilized in some cases because short electron escape depth in this method makes it possible to examine atomic and electron states of liquid surface and solid-liquid interfaces. In order to realize high efficiency measurements through the total electron yield method, high efficiency films with high electron transmission are a key and therefore have been strongly desired.

To construct our original device for the total electron yield measurements, we propose to utilize graphene which is atomically thin and has high electron transmission [1]. As the first step, we tried to establish our original experimental setup to verify our idea as shown in Fig. 1. As a preliminary experiment, liquid water was sandwiched by two silicon nitride windows with apertures of 0.5 x 0.5 and 0.2 x 0.2 mm instead of graphene. We successfully detected transmitted lights and photoelectrons as shown in Figs. 2 and 3, respectively.

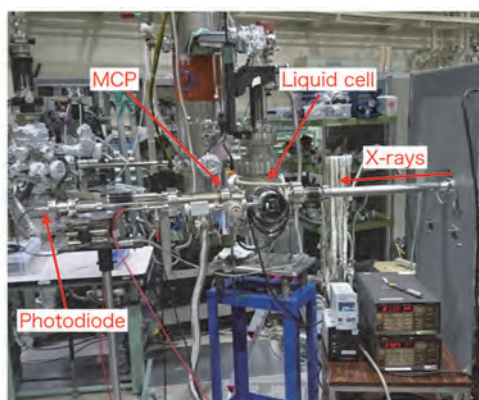


Fig. 1. Our original experimental setup for the high-efficient total electron yield method.

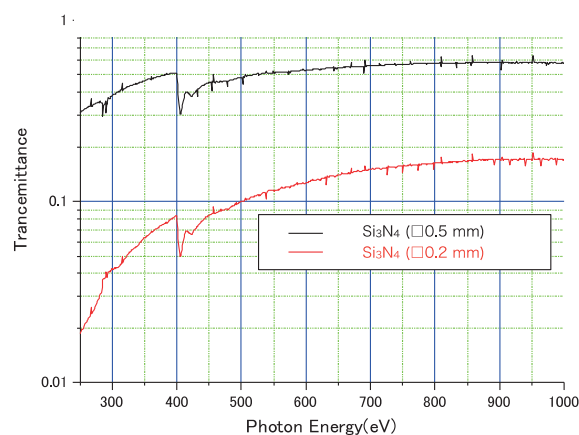


Fig. 2. Transmittance as a function of energy for the silicon nitride windows with aperture areas of 0.5 mm (black) and 0.2 mm (red).

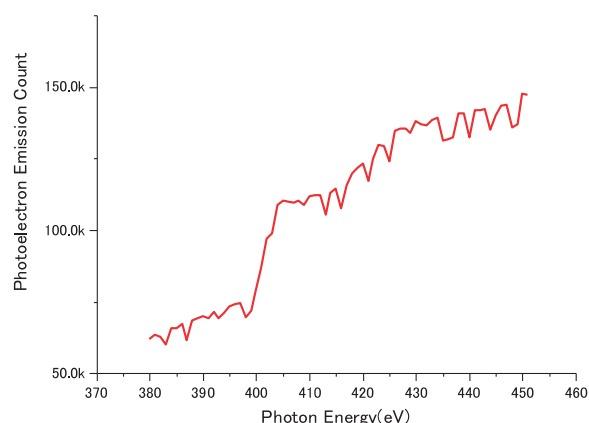


Fig. 3. Photoelectron count around the nitrogen edge structure.

[1] G. Hassink, R. Wanke, I. Rastegar, W. Braun, C. Stephanos, P. Herlinger, J. H. Smet and J. Mannhart, *APL Materials* **3** (2015).

BL5B

Development of Multilayer Coated Mirror for the Next Jupiter Mission

L. Huiyang¹, Y. Jie¹, S. Nishimura¹, K. Yoshioka^{1,2} and I. Yoshikawa^{1,2}

¹Department of Complexity Science and Engineering, Graduate School of Frontier Sciences, The University of Tokyo, Kashiwa 277-8561, Japan

²Department of Earth and Planetary Science, Graduate School of Science, The University of Tokyo, Tokyo 113-0033, Japan

Observation of solar planets in the extreme ultraviolet (EUV) spectral region is important to study dynamics of their magnetospheres. Recently, extension to shorter wavelength (XUV: x-ray and ultraviolet) is highly desired. However, there are still technical difficulties due to lack of techniques for collection of photons. Multilayer coated mirrors reflecting the XUV radiation at the normal incidence have potentials to overcome the difficulties [1].

Yoshikawa et al. (2005) showed the reflectivities of their newly developed multilayer coatings, consisting of 40 pairs of Mg and SiC [2]. The decrease in reflectivity was reported in high temperature (~55 °C) and high humidity (~65 %) environment. For science missions generally, science instruments have to survive high temperature and humidity environments. Therefore, we should develop robust instruments against environmental changes.

The measurement setup was illustrated in Figure 1. The B₄C/Mg-Si mirror was fixed on a L-shaped jig, and the L-shaped jig was mounted on the stage. Parallel movement by x,y motor and rotation by θ motor are possible.

The reflectivity is measured each 0.1 nm step from 25 nm to 35 nm. Figure 2 shows the reflectivity at different incident angles of the wavelength scan experiment before conducting the environmental test. Figure 3 shows the reflectivity of the wavelength scan experiment after conducting the environmental test. We conducted the environmental test in high temperature (50 °C) for 24 hours.

It can be seen from Fig. 2 that when the incident angle is 15 degrees and the wavelength is 31.6 nm, the reflectivity reaches its maximum, which is close to 30 %. On the other hand, Fig. 3 shows that after the environmental test, when the incident angle is 25 degrees and the wavelength is 29.2 nm, the reflectivity reaches its maximum value of 19 %, which is 2.4 nm shorter than the result before the environmental test.

[1] D.G. Stearns *et al.*, Multilayer mirror technology for soft-x-ray projection lithography, *Appl. Opt.* **32** (1993) 6952.

[2] Yoshikawa *et al.*, Characteristics of SiC/Mg multilayer mirrors, *Optics for EUV, X-Ray, and Gamma-Ray Astronomy II.* **59001A** (2005).

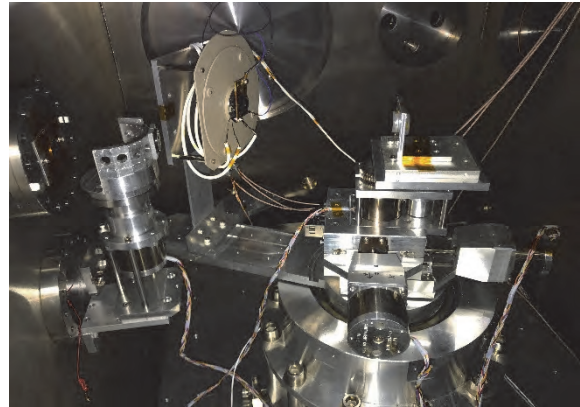


Fig. 1. Photo of the measurement setup.

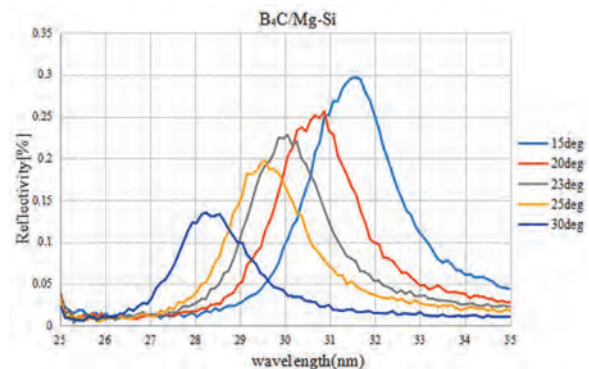


Fig. 2. Reflectivity of B₄C/Mg-Si multilayer mirror in a wavelength region 25-35 nm before conducting the environmental test.

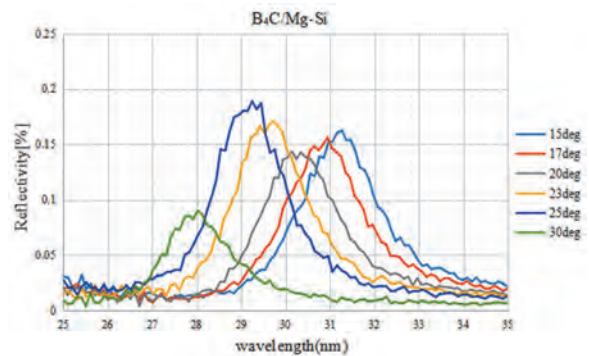


Fig. 3. Reflectivity of B₄C/Mg-Si multilayer mirror in a wavelength region 25-35 nm after conducting the environmental test.

BL5B

Performance Evaluation of Filaments used in the Hydrogen Absorption Cell

M. Kuwabara¹, K. Yoshioka², M. Taguchi³, Y. Suzuki⁴, S. Nishimura⁴ and T. Kosugi²

¹*Institute of Space and Astronautical Science, Japan Aerospace Exploration Agency, Sagamihara 252-5210, Japan*

²*Department of Complexity Science and Engineering, Graduate School of Frontier Sciences, The University of Tokyo, Kashiwa 277-8561, Japan*

³*College of Science, Rikkyo University, Tokyo 171-8501, Japan*

⁴*Department of Earth and Planetary Science, Graduate School of Science, The University of Tokyo, Tokyo 113-0033, Japan*

In the planetary exosphere, hydrogen atoms resonantly scatter the solar hydrogen Lyman-alpha radiation (121.567 nm) and form the hydrogen corona. Imaging observation of this emission provide us to obtain the spatial structure because of the dependency of its brightness on the number density of the hydrogen atoms.

An absorption cell technique is an efficient tool for the density and temperature measurements for the exospheric hydrogen atoms by remotely. Additionally, the absorption cell technique has some advantages over other instruments in terms of mass, size, and simplicity. Therefore, the absorption cell technique is suitable for future planetary exploration with small size spacecraft. See Kuwabara *et al.* [2018] for details on the principle of the absorption cell technique [1].

The absorptance of hydrogen Lyman-alpha radiation depends on the number of hydrogen atoms along the optical path in the absorption cell. The dissociation rate of hydrogen molecules depends on the surface area and temperature of the filament. In this experiment, therefore, we evaluated absorption performances of two filaments with different shapes by using the SOR beam with high intensity and stability. Table 1 shows the specifications of the filaments.

Figure 1 shows the configuration of the experiment. A hydrogen absorption cell imager consists of an absorption cell, MgF₂ band-pass filter, and photon detector. An assembly of microchannel plates (MCPs) and a resistive anode encoder (RAE) was used as the photon detector. The dependence of the absorptance of hydrogen Lyman-alpha radiation on the power consumption (i.e. filament temperature) was measured using each filament.

The result is shown in Fig. 2. The absorptance of hydrogen Lyman-alpha radiation when using the X10731 filament is higher than when using the X10478 filament. This is probably due to the large surface area of the X10731 filament. For the next step, further investigations such as long-term stability of absorption and durability of the filaments are required.

Table 1. Specifications of filaments.

	Cross-section	Coil length
X10478	Φ 48 μm	3 mm
X10731	11 x 61 μm	3 mm

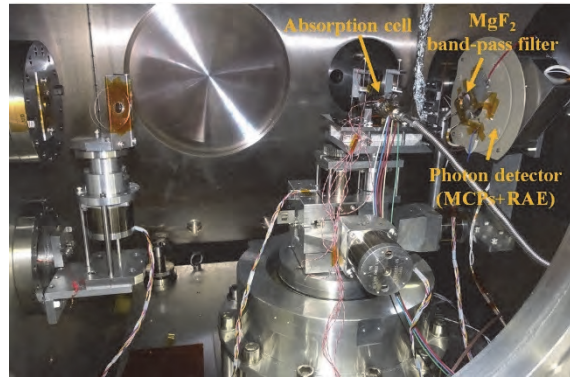


Fig. 1. Configuration of the experiment.

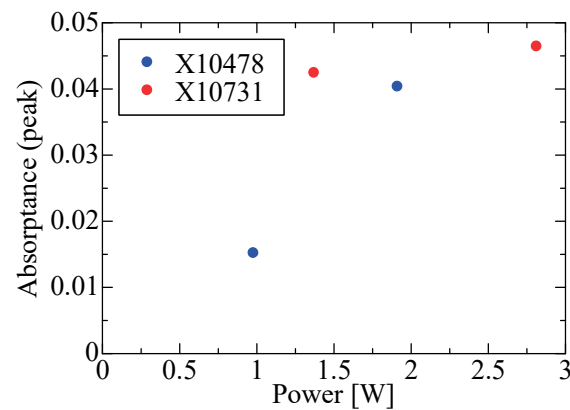


Fig. 2. Absorbance of the absorption cell.

[1] M. Kuwabara *et al.*, Review of Scientific Instruments **89** (2018) 023111.

BL5B

Trial to Mitigate Photon-Energy Drift of BL5B

H. Zen¹, E. Nakamura², K. Hayashi² and K. Tanaka^{2,3}

¹*Institute of Advanced Energy, Kyoto University, Uji 611-0011, Japan*

²*UVSOR Synchrotron Facility, Institute for Molecular Science, Okazaki 444-8585, Japan*

³*School of Physical Sciences, The Graduate University for Advanced Studies, SOKENDAI, Okazaki 444-8585, Japan*

The variation of the photon beam properties, such as beam position, photon energy, and so on, during user operation in the beamline is a big issue in synchrotron radiation (SR) facilities. A photon-energy drift at BL5B has been observed during user experiments [1]. We have started a detailed investigation of the source of the photon-energy drift. In 2019, we found that the M0 mirror, which is water cooled but directly illuminated with SR, in the beamline is not the major source of the energy drift but the M1 mirror could be the major source of that [2]. At that time, temperature of the M1 mirror holder was higher than the M1 mirror. This implied that the SR which was not reflected by the M0 mirror directly hit on the M1 mirror holder. At the same time, we found the correlation between the photon-energy drift and the temperature of the M1 mirror holder. We considered that the large temperature rise of the M1 mirror holder and heat induced deformation of it was the major source of the photon-energy drift.

In this fiscal year, a metallic mask was installed to avoid the SR directly hitting on the M1 mirror holder as shown in Fig. 1 left. In order to monitor the temperature of the mirror and mirror holder, four thermocouples (TCs) have been installed. For temperature stabilization of the mirror, a heater is installed at the center of the mirror. At first, effect of the mask was examined. The temperature variations of the M1 mirror and mirror holder with the mask are shown in Fig. 1 right. As the result, the temperature increased up to 35 deg. C in 36 hours with the mask. This was much smaller than the temperature rise without mask (up to 73 deg. C) [2]. The temperature rise of the mirror holder was greatly suppressed.

The photon-energy drift after the monochromator of BL5B was continuously monitored by using the absorption edge of an aluminum filter. Results are shown in Fig. 2 (a). The temperature of the mirror was stabilized by the feedback control of the heater power supply according to the temperature of the mirror center. Two temperature targets were examined in this test. One was the 60 deg. C, which was slightly higher than the saturated temperature of the mirror. The other was 80 deg. C, which was 20 deg. C higher than the saturated temperature of the mirror. Unfortunately, the photon-energy drift cannot be suppressed by installation of the mask and the temperature feedback of the M1 mirror. However, the photon-energy and the temperature of the mirror holder have same periodic variation and drift when the target temperature was set to 80 deg. C as one can see in Fig. 2 (b). This implies that the major source of the photon-energy drift is M1 mirror holder and not

M1 mirror itself.

To suppress the photon-energy drift of BL5B, temperature measurement points of M1 mirror holder should be increased and the most critical point must be found and temperature of the point must be stabilized.

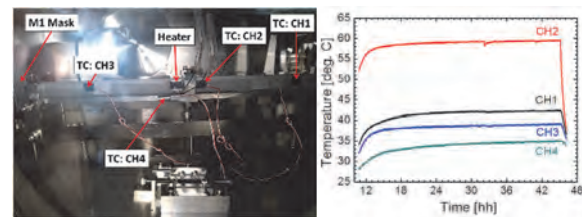


Fig. 1. (left) Photo of the M1 mirror and mirror holder with the mask, thermocouples (TCs) and a heater. (right) Temperature evolution during a SR irradiation for 36 hours with the M1 mask.

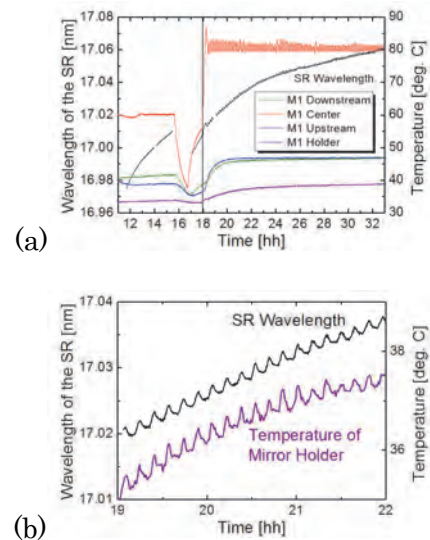


Fig. 2. (a) Measured photon-energy drift with temperature stabilization of M1 mirror. Up to 15:30, the target temperature of the feedback was 60 deg. C. From 18:00, the target temperature was 80 deg. C. (b) Closed up of 19-22 hour for SR wavelength and temperature of the mirror holder.

[1] K. Hayashi, UVSOR Activity Report 2011 **39** (2012) 121.

[2] H. Zen, UVSOR Activity Report 2019 **47** (2020) 42.

UVSOR User 4

